

# AN OPTIMUM DESIGN OF HIGH-POWER AMPLIFIER WITH HIGH EFFICIENCY USING A REALIZABLE HARMONIC LOADING CIRCUIT

Junghwan Moon, Jangheon Kim, Jungjoon Kim, Ildu Kim, and Bumman Kim

Department of Electrical Engineering, Pohang University of Science and Technology, Pohang, Gyeongbuk 790-784, Korea; Corresponding author: jhmoon@postech.ac.kr

Received 10 June 2009

**ABSTRACT:** An optimum design approach for a highly efficient power amplifier (PA) using a packaged high-power device is described. Large fundamental load impedance assisted by a simple second harmonic manipulation is explored to improve the efficiency when maintaining the power density. For demonstration of the performance, the PA is implemented using GaN HEMT device at 2.655 GHz. In the experiment, the fabricated PA achieves power-added efficiency (PAE) of 64.3% at the saturated output power of 49.2 dBm. For 802.16e mobile worldwide interoperability for microwave access signal, the PA delivers the PAE of ~31% and ACLR of -49 dBc at the 10 dB backed-off power of 40 dBm after the digital feedback predistortion linearization. © 2010 Wiley Periodicals, Inc. *Microwave Opt Technol Lett* 52: 818–822, 2010; Published online in Wiley InterScience (www.interscience.wiley.com). DOI 10.1002/mop.25032

**Key words:** efficiency; GaN HEMT; power amplifier (PA); worldwide interoperability for microwave access (WiMAX)

## 1. INTRODUCTION

Recently, the high power-added efficiency (PAE) of a power amplifier (PA) is regarded as an important design parameter for repeater and base station transmitters due to thermal management, reliability, cost, etc. For the enhanced PAE, switching or saturated mode PAs have been received a lot of attention. These PAs require the short and open impedances or proper capacitive and inductive values for harmonic components to shape the voltage and current waveforms at the current source of a transistor [1–6]. However, in case of the commercial packaged high-power device, manipulating the harmonic impedances at the current source is troublesome because the package effects, such as bonding wire and package capacitance, and internal matching not only prevent PAs from being controlled for the harmonic impedances but also reduce tolerance of the harmonic manipulation. Moreover, only limited harmonics, the second and/or third harmonics, can be controlled because the large output capacitance of a large periphery device leads to short impedances for higher harmonics [1], restricting the tunability. As a result, the

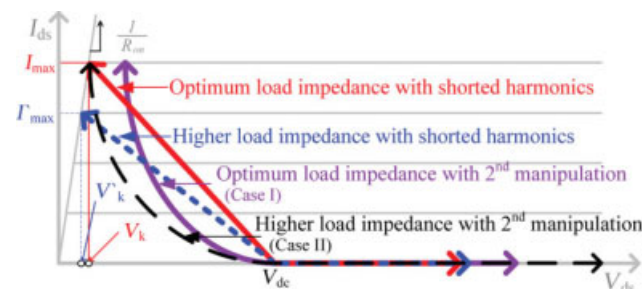


**Figure 1** Load lines for various load conditions. [Color figure can be viewed in the online issue, which is available at www.interscience.wiley.com]

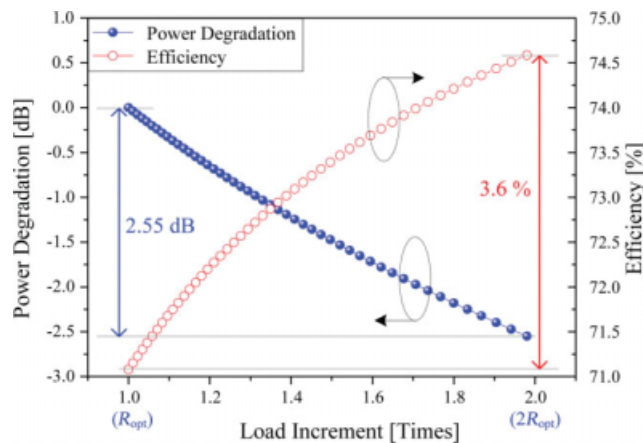


**Figure 2** Power degradation and efficiency increase according to the load increment. [Color figure can be viewed in the online issue, which is available at www.interscience.wiley.com]

conventional design approaches for a highly efficient PA should be readjusted when the packaged device is used.

In this article, we present an optimum design approach to realize a highly efficient PA using the high-power device. Increasing the fundamental load impedance and manipulation of the second harmonic component are investigated to improve both the PAE and output power. Moreover, high efficiency and linearity are achieved using the digital feedback linearization (DFBPD) technique at an average output power for mobile worldwide interoperability for microwave access (WiMAX) signal. From the experimental results, it is demonstrated that the proposed design approach not only leads to high performance but also is realizable.

## 2. AN OPTIMUM PA DESIGN USING A HIGH-POWER DEVICE

### 2.1. Manipulation of Fundamental Load Impedance

Figure 1 shows load lines according to the various load impedances ( $R_L$ ) with shorted harmonic impedances for a Class-B PA operation. For the power matching  $R_L = R_{opt}$  case (red solid line), the swings of the current and voltage reach to their maximum values, and its fundamental output power,  $P_{1,opt}$ , and efficiency,  $\eta_{opt}$ , are given by:

$$P_{1,opt} = \frac{I_{max}}{4} \cdot (V_{dc} - V_k) \quad (1)$$

$$\eta_{opt} = \frac{\pi}{4} \cdot \left(1 - \frac{V_k}{V_{dc}}\right) \times 100.$$

For a higher  $R_L$  case (blue dotted line), the maximum current is reduced by the higher  $R_L$  and the knee voltage is reduced by  $V'_k = R_{on} \cdot I_{max}$ . As a result, the maximum value of voltage swing is enlarged a little from  $(V_{dc} - V_k)$  to  $(V_{dc} - V'_k)$ , where  $R_{on}$  is the on-resistance. Thus, its fundamental output power is degraded significantly, whereas efficiency is increased only a little. Figure 2 shows the calculated power degradation and efficiency improvement according to the load increment, which is numerically performed using MATLAB. For the calculation, we assumed a  $V_{dc}$  of 29 V,  $I_{max}$  of 19 A, and  $R_{on}$  of 0.14  $\Omega$  with a uniform transconductance.

### 2.2. Second Harmonic Manipulation

The voltage swing of the PA is limited by the knee voltage rather than the drain-to-source breakdown voltage because the supply voltage is, usually, near to the knee voltage. The

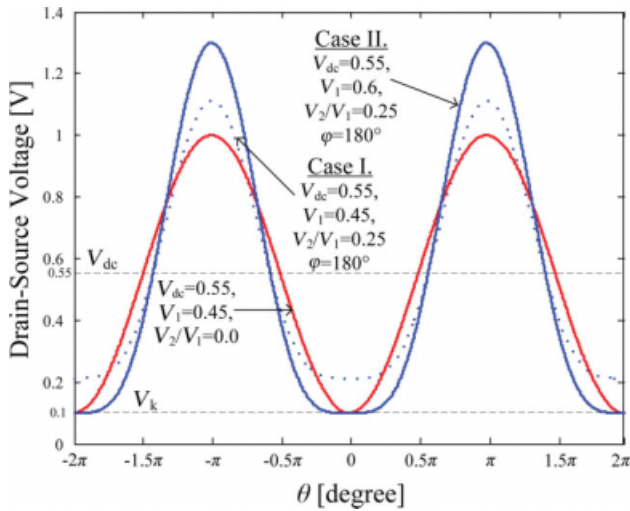


**Figure 3** Drain voltage waveforms with second harmonic component. [Color figure can be viewed in the online issue, which is available at [www.interscience.wiley.com](http://www.interscience.wiley.com)]

maximum magnitude of the voltage waveform is constrained by  $(V_{dc} - V_k)$  when all harmonics are shorted at the output current source of the device [2]. If the voltage waveform is manipulated by the second-order harmonic with a proper magnitude and phase, the lower side of the waveform can be flattened and the upper side is peaked, which has a potential of increasing the fundamental voltage component over the value indicated by the device physical limitations,  $V_{dc} - V_k$ . The voltage waveform with the second harmonic component is given by:

$$V_{ds}(\theta) = V_{dc} - V_1 \cdot \cos(\theta) - V_2 \cdot \cos(2\theta + \varphi), \quad (2)$$

where  $V_{dc}$ ,  $V_1$ , and  $V_2$  are magnitudes of the DC, fundamental, and second harmonic voltages, respectively.  $\varphi$  is phase of the second harmonic voltage.

Figure 3 shows the various voltage waveforms manipulated by the second harmonic component. Here, the maximally flat condition at the lower part is achieved with  $V_2/V_1 = 0.25$  and  $\varphi = 180^\circ$ . If the voltage waveform does not have any second harmonic, i.e., all harmonics are short, the voltage waveform should be sinusoidal and its magnitude is  $(V_{dc} - V_k)$  represented by red solid line in Figure 3. Because of the addition of the second harmonic makes the waveform horizontally asymmetrical, the lower part of the affected waveform is flattened and has higher value than uninfluenced one (Case I). In this case, however, there is no performance improvement because the fundamental voltage is not increased due to the same load impedance and DC bias is also identical: No power increase or PAE enhancement. If the fundamental voltage is increased using larger  $R_L$ , whereas the ratio of  $V_2$  and  $V_1$  is maintained to be 0.25, the waveform can be increased until the lower part reaches the knee voltage, which is depicted by blue solid line (Case II). Because of the increment of the fundamental voltage component and decrement of the non-zero voltage region both the output power and efficiency can be improved. In this case, the DC power is the same as the optimum Class-B PA, whereas the RF power is increased. Thus, the PAE is increased. The load lines for the Case I and Case II are illustrated in Figure 1, showing that the Case II is the optimum for Class-B PA operation with the second harmonic manipulation.

In this simulation, we assume that the second harmonic voltage is out-of-phase with respect to the fundamental component.

In practical case, however, it is difficult to satisfy the magnitude and phase conditions of the second harmonic because the package parasitic and internal matching in the high-power device do not allow accurate control of the harmonic component. If the second harmonic is added improperly, it is deleterious rather than beneficial to the performance of the PA. Therefore, we need a circuit topology with a large tolerance for the second harmonic control and the required harmonic impedance should be realizable. Figure 4 shows the fundamental voltage gain according to the  $V_2/V_1$  and  $\varphi$ . When  $V_2/V_1$  and  $\varphi$  are 0.35 and  $180^\circ$ , the maximum voltage increment could be achieved, 1.4142. As indicated in Figure 4, the region for the second harmonic with the voltage gain is very wide, about 25% of the total variations, and the large tolerance allows easy control of the second harmonic.

Also, the large  $R_L$  allows the PA to generate a large amount of the harmonic current, decreasing the magnitude of the required harmonic load impedance [2]. In the high-efficiency PA design using high-power packaged device, lowering the needed harmonic load impedance is beneficial because the package effects and large output capacitance make it difficult to deliver the large harmonic impedance at the internal current source. From these investigations, we can conclude that the proposed approach is more practical and realizable than conventional ones.

### 3. IMPLEMENTATION AND EXPERIMENTAL RESULTS

To validate the design concept of the high-efficiency PA using a packaged high-power device by using the large fundamental load impedance and controlling the second harmonic component, the PAs are fabricated using Nitronex GaN HEMT NPT25100 devices with 100-W peak envelop power (PEP) at 2.655 GHz operating frequency. For comparison, we have implemented three kinds of PAs with: (1) the optimum fundamental load impedance for maximum output power, (2) the higher fundamental load impedance for increasing the efficiency, and (3) the higher fundamental load impedance employing the second harmonic control for increasing the power and efficiency performances.

In the experiments, we have observed the gain and output power performances according to the external load impedance because we cannot see the fundamental load impedance at the current source of the transistor. The second harmonic is

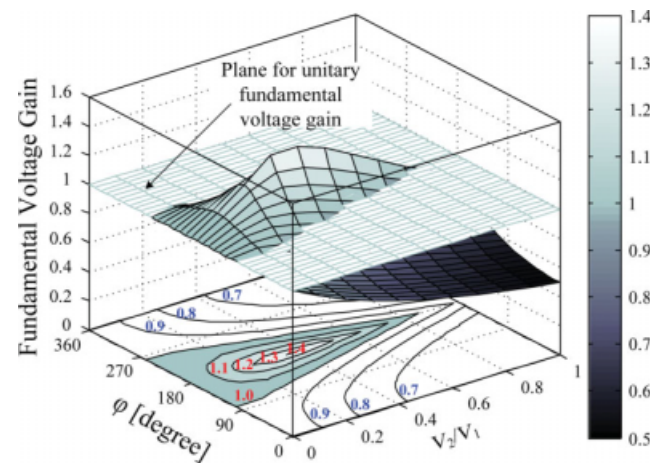
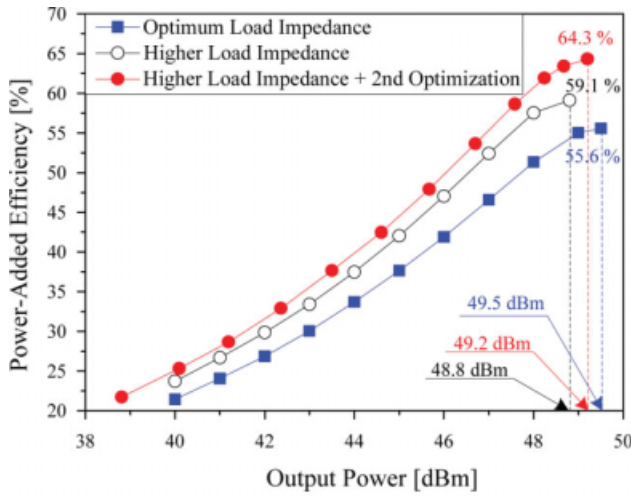
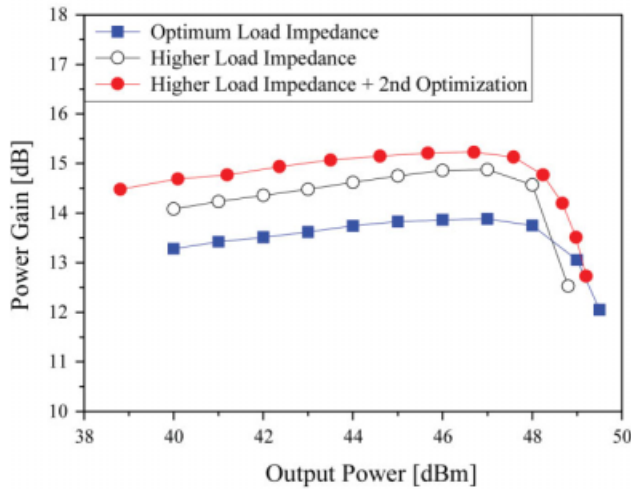


**Figure 4** Fundamental voltage gain according to the  $V_2/V_1$  and  $\varphi$ . [Color figure can be viewed in the online issue, which is available at [www.interscience.wiley.com](http://www.interscience.wiley.com)]



(a)



(b)

**Figure 5** Measured performances of the amplifiers: (a) PAE, (b) Gain. [Color figure can be viewed in the online issue, which is available at [www.interscience.wiley.com](http://www.interscience.wiley.com)]

manipulated on the drain bias line, which is attached at the drain lead, and the matching circuit, which does not have any special harmonic loading circuit because the second harmonic impedance is not necessarily large due to the high second harmonic current generated from the large  $R_L$  matching. The fundamental and second harmonic load impedances are iteratively readjusted to optimize the PAE performance in the experiment.

Figures 5(a) and 5(b) show the measured PAE and gain performances of the implemented PAs. The PA with optimum fundamental load has PAE of 55.6% at 49.5 dBm of  $P_{\text{sat}}$ . Because the large fundamental load impedance with shorted harmonic reduces the maximum current and knee effect, the PAE of the PA using large load is increased, but the  $P_{\text{sat}}$  is decreased. How-

**TABLE 1** Measured Performances for the Implemented PAs

	$P_{\text{sat}}$ (dBm)	Gain (dB)	PAE (%)
PA with optimum load	49.5	12.1	55.6
PA with higher load	48.8	12.5	59.1
PA with higher load + second opt.	49.2	12.7	64.3

**TABLE 2** Performance Comparison of High-Power/Efficiency PAs

References	$f_0^a$ (GHz)	$P_{\text{sat}}$ (W)	PAE (%)	$V_{\text{dd}}$ (V)	Class
[3] <sup>b</sup>	2.14	100	70.3	50	E
[4] <sup>b</sup>	2.6	148	59	50	AB
[5]	2.14	156	58.5	28	AB
[6]	2.14	63	57.2	28	AB
This work	2.655	83.17	64.3	29	AB

<sup>a</sup>  $f_0$  denotes the operating frequency.

<sup>b</sup> Output internal matching circuit is optimized to maximize the PAE.

**TABLE 3** Linearization Performance at an Average Output Power of 40 dBm (31.2%) for Mobile WiMAX Signal

	ACLR (dBc) at $\pm 7$ -MHz Offset	RCE (dB)
Before linearization	-28.7/-26.3	-21.7
After linearization	-49.0/-51.2	-43.0

ever, the proposed PA achieves the PAE improvement of around 10%, whereas the output power is nearly maintained at the same level of the PA with optimum fundamental load. If the second harmonic is accurately added to obtain the maximum fundamental voltage, both the output power and PAE will be increased. The measured PAE, gain, and  $P_{\text{sat}}$  performances are summarized in Table 1. The performances of the implemented PA are compared with the other published data using GaN HEMT with operating frequency of above 2 GHz and  $P_{\text{sat}}$  of more than 50 W in Table 2. These experimental results show clearly that the proposed design concept is easily applicable for realizing a PA, using a high-power packaged device, with efficiency and power density.

To explore nonlinearity of the proposed PA, the mobile WiMAX-modulated signal is used, and the implemented PA is linearized using the DFBPD linearization technique to meet the linearity specification [7, 8]. Figure 6 shows the measured WiMAX spectra of the PA before and after linearization. The ACLR at an offset of 7 MHz is -49 dBc, which is an improvement of  $\sim 23$  dB at an average output power of 40 dBm. The PAE of the PA is  $\sim 31\%$  at the average output power. Figure 7 shows the measured AM/AM and AM/PM characteristics before

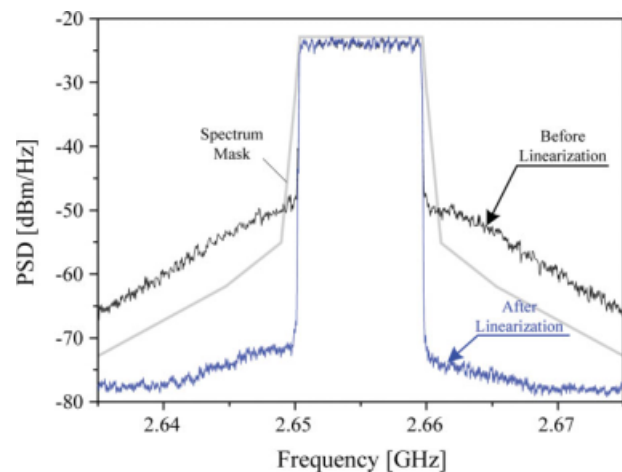


**Figure 6** Measured mobile WiMAX spectra before and after linearization at an average output power of 40 dBm. [Color figure can be viewed in the online issue, which is available at [www.interscience.wiley.com](http://www.interscience.wiley.com)]

and after linearization at the same average output power. The relative constellation error (RCE) is  $-43$  dB, which is an improvement of  $\sim 21.3$  dB, as shown in Figure 8. It is shown that the proposed PA delivers high efficiency with an acceptable linearity, which can be linearized to the level suitable for the linear power amplifier (LPA). The results are summarized in Table 3.

#### 4. CONCLUSIONS

In this article, an optimum design method for highly efficient PA using a packaged high-power device is presented. The design shortcomings of the harmonic-controlled PA in the high-power device are discussed. The large fundamental load impedance with a simple second harmonic manipulation increases the output power and efficiency because it enlarges the fundamental voltage but reduces the non-zero voltage region. The only sec-

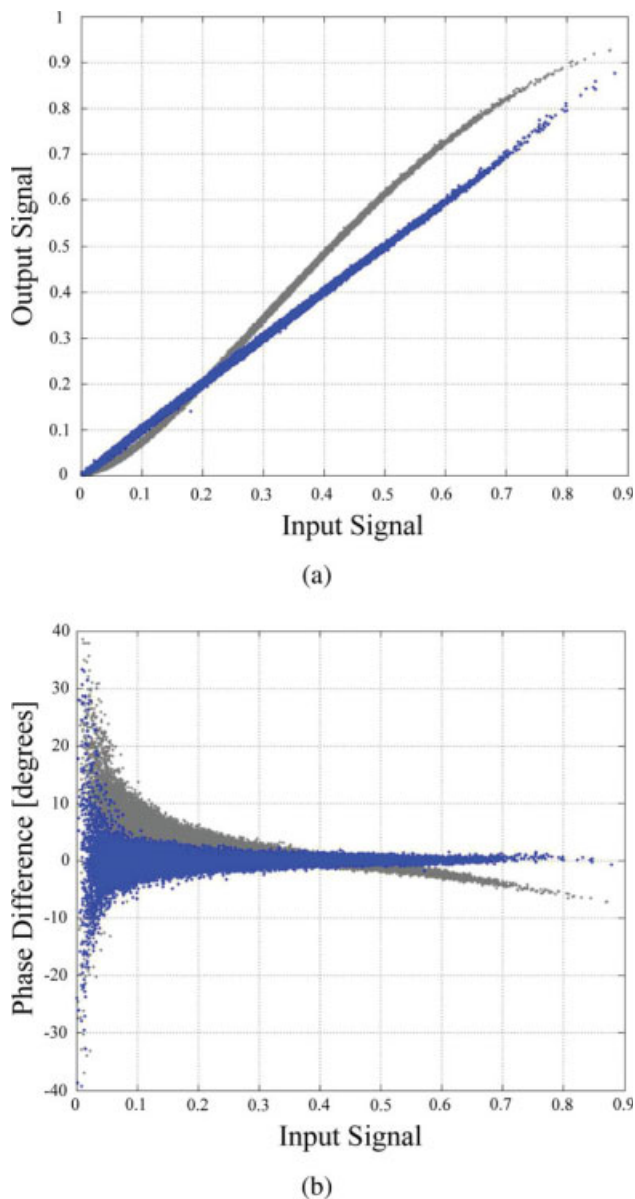


**Figure 7** Measured (a) AM/AM and (b) AM/PM characteristics before (gray) and after (blue) linearization at an average output power of 40 dBm. [Color figure can be viewed in the online issue, which is available at [www.interscience.wiley.com](http://www.interscience.wiley.com)]

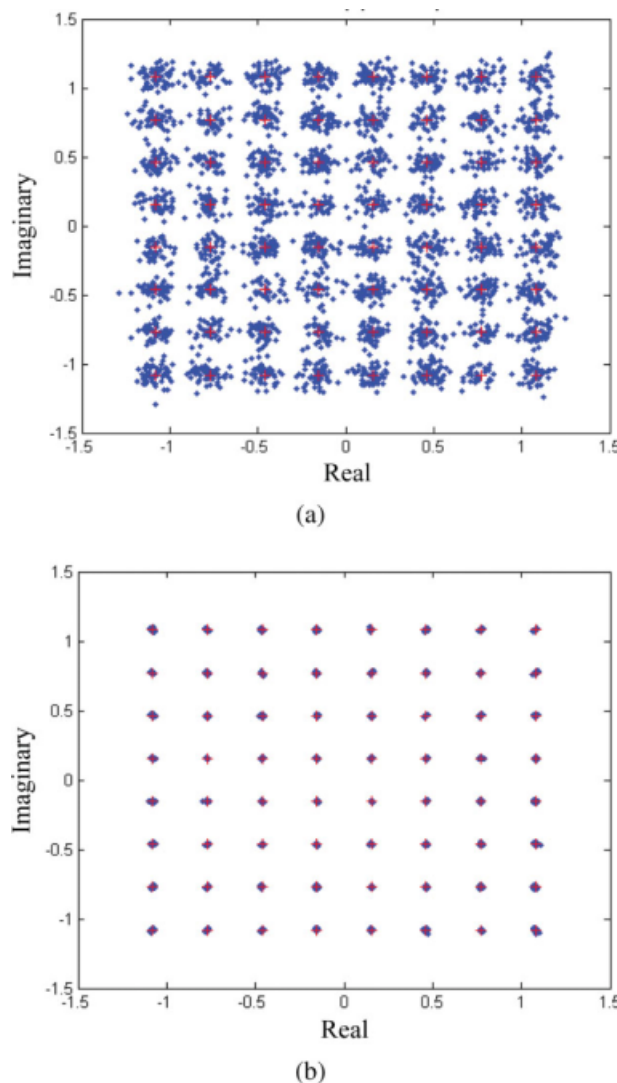


**Figure 8** Measured constellation diagram at an average output power of 40 dBm. (a) Before linearization; (b) after linearization. [Color figure can be viewed in the online issue, which is available at [www.interscience.wiley.com](http://www.interscience.wiley.com)]

ond harmonic termination approach is quite tolerable and realizable. For demonstration, the PA is designed using Nitronex 100-W PEP GaN HEMT NPT25100 at 2.655 GHz, and PAE of 64.3% is achieved at  $P_{\text{sat}}$  of 49.2 dBm. For the mobile WiMAX signal, the PA delivers the PAE of  $\sim 31\%$  and ACLR of  $-49$  dBc at the 10 dB backed-off power of 40 dBm after the DFBDP linearization. Experimental results allow us to conclude that the proposed design approach is an appropriate method for realizing a highly efficient PA using a packaged high-power device.

#### ACKNOWLEDGMENTS

This work was supported by ETRI SoC Industry Promotion Center, Human Resource Development Project for IT SoC Architect, and WCU (World Class University) program through the Korea Science and Engineering Foundation funded by the Ministry of Education, Science and Technology (Project No. R31-2008-000-10100-0).

#### REFERENCES

1. S.C. Cripps, RF power amplifiers for wireless communications, 2nd ed., Artech House, Norwood, MA, 2006.

2. P. Colantonio, F. Giannini, G. Leuzzi, and E. Limiti, High efficiency low-voltage power amplifier design by second-harmonic manipulation, *Int J RF Microw Comput-Aided Eng* 10 (2000), 19–32.
3. N. Ui and S. Sano, A 100W class-E GaN HEMT with 75% drain efficiency at 2GHz, *Proceedings of European Microwave Conference*, Manchester, England 2006, pp. 72–75.
4. H. Sano, N. Ui, and S. Sano, A 40W GaN HEMT Doherty power amplifier with 48% efficiency for WiMAX applications, *Compound Semiconductor Integrated Circuit Symposium*, 2007; [CD ROM].
5. W. Nagy, S. Singhal, R. Borges, J.W. Johnson, J.D. Brown, R. Therrien, A. Chaudhari, A.W. Hanson, J. Riddle, S. Booth, P. Rajagopal, E.L. Piner, and K.J. Linthicum, A 150W GaN-on-Si RF power transistor, *IEEE MTT-S Int Microwave Symp Dig*, Long Beach, CA (2005), 483–486.
6. R. Vetur, Y. Wei, D.S. Green, S.R. Gibb, T.W. Mercier, K. Leverich, P.M. Garber, M.J. Poulton, and J.B. Shealy, High power, high efficiency, AlGaIn/GaN HEMT technology for wireless base station applications, *IEEE MTT-S Int Microwave Symp Dig*, Long Beach, CA (2005), 487–490.
7. Y.Y. Woo, J. Kim, J. Yi, S. Hong, I. Kim, J. Moon, and B. Kim, Adaptive digital feedback predistortion technique for linearizing power amplifiers, *IEEE Trans Microwave Theory Tech* 55 (2007), 932–940.
8. J. Kim, C. Park, J. Moon, and B. Kim, Analysis of adaptive digital feedback linearization techniques, *IEEE Trans Circuits Syst I*, in press.

© 2010 Wiley Periodicals, Inc.

## FREQUENCY AND TEMPORAL COHERENCE PROPERTIES OF DISTRIBUTED BRAGG REFLECTOR LASER

Jian Hong Ke, Ning Hua Zhu, Hong Guang Zhang, Jiang Wei Man, Ling Juan Zhao, Wei Chen, Xin Wang, Yu Liu, Hai Qing Yuan, Liang Xie, and Wei Wang

State Key Laboratory on Integrated Optoelectronics, Institute of Semiconductors, CAS, Beijing 100083, China; Corresponding author: nhzhu@semi.ac.cn

Received 10 June 2009

**ABSTRACT:** This article presents the investigation of frequency and temporal coherence properties of distributed Bragg reflector laser. In this scheme, a square-waveform voltage is applied to the phase section of the laser to tune optical wavelength, and delayed optical heterodyne technique is used for the analysis of spectral characteristics. Experiments show that lightwaves emitted from the same active region asynchronously are partially frequency and temporal coherent. When the two wavelengths are closer, the two waves are strongly coherent, and the coherence properties get weak as the delay time increases. © 2010 Wiley Periodicals, Inc. *Microwave Opt Technol Lett* 52: 822–825, 2010; Published online in Wiley InterScience (www.interscience.wiley.com). DOI 10.1002/mop.25031

**Key words:** distributed Bragg reflector laser; frequency coherence; optical heterodyning

### 1. INTRODUCTION

Frequency coherence as a new concept has been proposed recently [1]. It describes the field correlations between two lightwaves with different frequencies. For the coherent beams, the maximal intensity of the mixed beams may exceed the sum of the intensities of the beams [2], and the beat signal between the two beams would have a linewidth much narrower than the sum of the beam linewidths. These discrepancies in intensity and

linewidth are the most important features to describe the coherence properties of the lightwaves [1]. The study on frequency coherence is helpful for the deep understanding of the internal properties of lightwaves and generation of narrow linewidth and stable microwave signals. Narrow linewidth and high stability are desirable in many applications, such as communications, radar, and other military and commercial fields [3–6]. For example, using microwave signal produced on a photodetector in optical heterodyne scheme to measure frequency responses of wideband photodetectors has drawn great attention. Distributed Bragg reflector (DBR) laser is used in the improved heterodyne scheme due to its wavelength tunable property. It has been found that the linewidth of beat signal varies as tuning square-wave voltage, and calibration is inevitable to remove the influence of linewidth change and improve measurement accuracy [7]. However, linewidth of beat signal is closely related to the frequency coherence of two lightwaves, which has been studied in our previous work [1]. Therefore, frequency coherence is extremely important to obtain a narrow linewidth and stable microwave signal. Up to now, frequency coherence properties of lightwaves from a DBR laser have never been studied.

In this article, we investigate frequency and temporal coherence properties of lightwaves emitted from a DBR laser asynchronously. Delayed optical heterodyne technique is used to analyze the linewidths of the lightwaves generated at different time.

### 2. FREQUENCY COHERENCE

#### 2.1. Experimental Setup

The experimental setup is shown in Figure 1. A square-waveform voltage generated from a waveform generator (Agilent 33250A) was applied to the phase section of the DBR tunable laser to tune its wavelength. Wavelengths  $\lambda_1$  and  $\lambda_2$  correspond to the high voltage  $V_H$  and low voltage  $V_L$  of the waveform, respectively, with a time interval of  $\tau$  (half period of the square waveform). A 270- $\Omega$  resistor was inserted in between the waveform generator and the DBR laser to limit the tuning current. Lightwave at  $\lambda_3$  from another narrow linewidth tunable lightwave source (Agilent 8164B) was used as reference light. These lightwaves were launched into a Mach-Zehnder interferometer with an erbium-doped fiber amplifier (EDFA) in the fiber delay path. The EDFA was used to compensate fiber loss and would not change the light properties. A polarization controller PLC-003-S-90 from General Photonics was used. The output lightwaves were divided into two paths. One was measured by an optical spectrum analyzer (OSA, Advantest Q8384), and the other was detected by an 18-GHz photodetector (Agilent 11982A), and then its spectrum was measured by a spectrum analyzer (ESA, Advantest R3182).

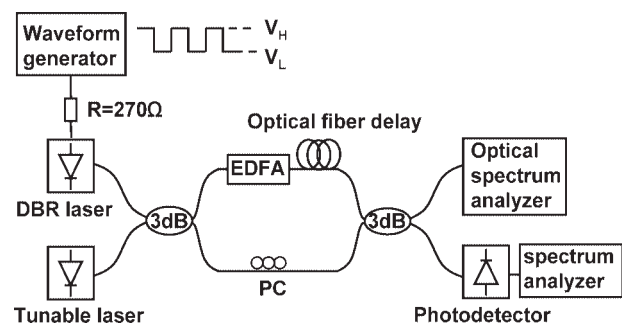


Figure 1 Experimental setup